PHYSICAL REVIEW B VOLUME 1, NUMBER 10 15 MAY 1970

Jahn-Teller Effect on the Structure of the Emission Produced by Excitation in the A Band of KI:Tl-Type Phosphors. Two Kinds of Minima on the $\Gamma_4^-(^3T_{1u})$ Adiabatic Potential-Energy Surface*

ATSUO FUKUDA
The Institute for Solid State Physics, The University of Tokyo, Minato-ku, Tokyo, Japan
and
Argonne National Laboratory,† Argonne, Illinois 60439

(Received 27 October 1969)

Emission spectra, excitation spectra, and decay times of Ga^+, In^+, and Tl^+ in KI, KBr, KCl, and NaCl have been investigated at 1.8–300°K under excitation in the A-absorption band. There are three types of temperature variation of the emission spectra; these types are represented by KI:Tl, KBr:Tl, and KCl:Tl, respectively. In case of types (1) and (2), two emission bands, A_T (high energy) and A_X (low energy), are observed. The excitation spectrum for the A_T emission is slightly different from that for the A_X emission. The decay times of the A_X emission are complex and temperature dependent, as exemplified in KI:Ga and KI:In. The A_T emission is surely due to the inverse process of the A absorption, $\Gamma_4^-(^3T_{1u}) \rightarrow \Gamma_1^+(^1A_{1g})$. Four reasons are given why the A_X emission is not due to the inverse process of the D absorption as proposed by Illingworth and supported by Donahue and Teegarden. To explain the A_X emission, the Jahn-Teller effect on the $^3T_{1u}$ state has been considered by assuming Russell-Saunders coupling. Since the correlation of polarization indicates the existence of tetragonal minima, adiabatic potential-energy surfaces (APES's) in the $E_g(Q_2,Q_3)$ configuration coordinate space have been obtained for the $\Gamma_4^-(^3T_{1u})$ and $\Gamma_1^-(^3T_{1u})$ states. When the spin-orbit interaction is of suitable value as compared with the Jahn-Teller (electron-lattice) interaction, the obtained APES's have two kinds of minima. Emission is considered to occur from these minima to the ground state, at least at low temperatures. The APES's can explain why there exist the three types of the emission spectra as well as the characteristic features of the emission spectra, excitation spectra, decay times, and polarization. The importance of these APES's for analyzing the stress, Stark, and Zeeman effects on the A_T and A_X emission is pointed out.

I. INTRODUCTION

FOR broad absorption bands of centers in crystals, it is generally accepted that the Jahn-Teller effect (JTE) in an excited E or T state causes the splitting or structure of the absorption ($A \rightarrow E$ or T) band.[1–5] It is certain that the JTE alone can produce the splitting or structure[1,3–5] although in some cases, e.g., in the F center of cesium halides, the spin-orbit interaction also plays an important role for the splitting or structure.[2,4] At first thought, however, the JTE alone in the excited state does not seem to cause the splitting or structure of the corresponding emission (E or $T \rightarrow A$) band.[1,6,7] There exists only one kind of minima on the E or T adiabatic potential-energy surface (APES), unless the effect of spin-orbit interaction or of the proximity of other electronic states is taken into account.[8] If splitting or structure of the emission band is to be observed, the APES ought to have at least two kinds of minima.[7–9] According to the theoretical analysis made by Öpik and Pryce[8] and also by Kamimura and Sugano,[9] the $\Gamma_4^-(^3T_{1u})$ APES may have two kinds of minima if the spin-orbit interaction is of suitable value as compared with the Jahn-Teller interaction. As far as the author is aware, however, there exists no trustworthy experimental evidence which enables us to conclude decisively that the splitting or structure of an emission band is certainly caused by the JTE in the excited state. It is interesting, therefore, to investigate experimentally whether the JTE together with the spin-orbit interaction in an excited state can really produce the splitting or structure of the emission band.

As a convenient system for the investigation of such an effect, one can point out Tl^+-type impurity centers, i.e., Ga^+, In^+, Tl^+, Ge^{2+}, Sn^{2+}, and Pb^{2+} centers, in alkali halides.[10] Analysis of the absorption spectra firmly established that they have the $^1A_{1g}(\Gamma_1^+)$ ground state and the three excited states, $^3T_{1u}(\Gamma_1^-, \Gamma_4^-, \Gamma_3^-,$ and $\Gamma_5^-)$, $^1T_{1u}(\Gamma_4^-)$, and the perturbed exciton (Γ_4^-); the $^1T_{1u}$ and $^3T_{1u}$ excited states are well described by the molecular orbitals (MO's), a_{1g} and t_{1u}.[11–14] Transi-

* Work partially supported by U. S. Atomic Energy Commission.
† Present address.

[1] H. C. Longuet-Higgins, U. Öpik, M. H. L. Pryce, and R. A. Sack, Proc. Roy. Soc. (London) **A244**, 1 (1958).
[2] P. R. Moran, Phys. Rev. **137**, A1015 (1965).
[3] Y. Toyozawa and M. Inoue, J. Phys. Soc. Japan **20**, 1289 (1965); **21**, 1663 (1966).
[4] K. Cho, J. Phys. Soc. Japan **25**, 1372 (1968).
[5] A. Fukuda, J. Phys. Soc. Japan **27**, 96 (1969).
[6] W. B. Fowler, in *Physics of Color Centers*, edited by W. B. Fowler (Academic, New York, 1968), p. 145.
[7] A. Fukuda, S. Makishima, T. Mabuchi, and R. Onaka, J. Phys. Chem. Solids **28**, 1763 (1967).
[8] U. Öpik and M. H. L. Pryce, Proc. Roy. Soc. (London) **238**, A425 (1957).
[9] H. Kamimura and S. Sugano, J. Phys. Soc. Japan **14**, 1612 (1959).
[10] N. E. Lushchik and Ch. B. Lushchik, Opt. i Spektroskopiya **8**, 839 (1960) [Opt. Spectry. (USSR) **8**, 441 (1960)].
[11] S. Sugano, J. Chem. Phys. **36**, 122 (1962).
[12] A. Fukuda, Sci. Light (Japan) **13**, 64 (1964).
[13] A. Fukuda, K. Inohara, and R. Onaka, J. Phys. Soc. Japan **19**, 1274 (1964).
[14] T. Mabuchi, A. Fukuda, and R. Onaka, Sci. Light (Japan) **15**, 79 (1966).

tions $\Gamma_1^+(^1A_{1g}) \rightarrow \Gamma_4^-(^3T_{1u})$, $\Gamma_1^+(^1A_{1g}) \rightarrow \Gamma_4^-(^1T_{1u})$, and $\Gamma_1^+(^1A_{1g}) \rightarrow \Gamma_4^-$ (perturbed exciton) cause the well-known absorption bands, *A*, *C*, and *D*, respectively. The *A*- and *C*-absorption bands clearly show the splitting or structure due to the JTE in the excited states.[3–5] The structure of the *C* band is rather symmetric, while that of the *A* band is remarkably asymmetric.[3,5,12–14] The asymmetry indicates that the APES of the *A* excited state $\Gamma_4^-(^3T_{1u})$ is strongly modified by the spin-orbit interaction.[3,5] Hence splitting or structure of the emission band $\Gamma_4^-(^3T_{1u}) \rightarrow \Gamma_1^+(^1A_{1g})$ is expected.[8,9]

The emission spectra of Tl^+ centers in alkali halides were first measured as early as in 1930 by von Meyeren,[15] who found that excitation in the *A*-absorption band produces two emission bands at least in KBr:Tl and RbCl:Tl. Recently, Edgerton and Teegarden[16] have confirmed von Meyeren's result that the two emission bands are really excitable in the *A*-absorption band in KBr:Tl and KI:Tl. Similar results have also been obtained in NaI:Tl by Fontana *et al.*,[17] in NaCl:Ga by Mabuchi *et al.*,[14] in RbCl:Tl and RbBr:Tl by Inohara,[18] and in KBr:In by Fukuda *et al.*[7,19] In case of Sn^{2+} and Pb^{2+}, Zazubovich *et al.*,[20] Zazubovich and Kuketaev,[21] and also Fukuda *et al.*[7,19] observed that the two emission bands are excitable in the *A* absorption, and that excitation spectra for the two emission bands are completely different from each other even within the *A*-absorption band.

Four explanations have been given for the two emission bands and are summarized in Table I. Explanation (a) seems implorable, because the radiative lifetime of the excited state responsible for the low-energy emission band is less than 5×10^{-8} as determined by Illingworth.[22] Static causes in explanation (c) include an off-center position of the impurity ion, a covalent bonding between the impurity ion and the surrounding negative ion, and the existence of some defects close to the impurity ion. Various authors have considered that the JTE in an excited state belongs to explanation (c). However, there exists essential difference between explanations (b) and (c). In explanation (c) the symmetry of the center is considered to be less than cubic even in the ground state, while in explanation (b) the symmetry is considered to be cubic in the ground state. Moreover, the JTE alone in the excited state cannot explain two emission bands as mentioned above. Since the structure of absorption band[3–5,12–14] and the correlation of polarization[7,19] indicate that at least the symmetry of monovalent impurity-ion (Ga^+, In^+, and Tl^+) centers is rather cubic in the ground state, explanation (c) seems improbable except in the case of divalent impurity-ion (Sn^{2+} and Pb^{2+}) centers. Hence either (b) or (d) will be the probable explanation for the two emission bands at least in the case of monovalent impurity-ion (Ga^+, In^+, and Tl^+) centers.

TABLE I. Four explanations for the two emission bands, A_T and A_X, excitable in the *A*-absorption band.

	Excited state responsible for the low-energy emission (A_X)	Excited state responsible for the high-energy emission (A_T)	References
(a)	$\Gamma_1^-(^3T_{1u})$	$\Gamma_4^-(^3T_{1u})$	16
(b)	Component of the Jahn-Teller split $\Gamma_4^-(^3T_{1u})$	Component of the Jahn-Teller split $\Gamma_4^-(^3T_{1u})$	7, 9, 24–26
(c)	Component of $\Gamma_4^-(^3T_{1u})$ split by static causes	Component of $\Gamma_4^-(^3T_{1u})$ split by static causes	20, 21
(d)	An excited state of the I^- ions surrounding the Tl^+ impurity ion (an exciton perturbed by an adjacent impurity ion)	$\Gamma_4^-(^3T_{1u})$	22, 23

The purpose of the present paper is to report the emission spectra at various temperatures under excitation in the *A*-absorption band of Ga^+ and In^+ centers in several alkali halides and to demonstrate how well the JTE within the $a_{1g}t_{1u}$ electron configuration can explain the observed features of the emission spectra. In Sec. II are presented rather systematic data on the emission spectra of Ga^+ and In^+ in KI, KBr, KCl, and NaCl, and preliminary data on Sn^{2+} in KI and KBr. It becomes clear that the emission spectra of Ga^+ and In^+ are quite similar to those of Tl^+. Four reasons are given in Sec. III why explanation (d) is improbable. The JTE in the $^3T_{1u}$ state is explained in Sec. IV, where special attention is paid to the fact that there may exist two kinds of minima on the $\Gamma_4^-(^3T_{1u})$ APES. Finally, in Sec. V several luminescent properties concerning the emission spectra excitable in the *A*-absorption band are summarized and are explained in terms of the JTE and the spin-orbit interaction.

II. EMISSION SPECTRA AT VARIOUS TEMPERATURES EXCITED IN *A*-ABSORPTION BAND

Although there exist much emission data on Tl^+ centers, emission data on other Tl^+-type centers are

[15] W. von Meyeren, Z. Physik **61**, 321 (1930).
[16] R. Edgerton and K. Teegarden, Phys. Rev. **129**, 169 (1963); **136**, A1091 (1964).
[17] M. P. Fontana, W. J. Van Sciver, and H. Blume, Proceedings of the International Symposium on Color Centers in Alkali Halides, Rome, 1968 (unpublished), p. 99.
[18] K. Inohara, Sci. Light (Japan) **14**, 92 (1965).
[19] A. Fukuda, S. Makishima, T. Mabuchi, and R. Onaka, *Proceedings of the International Conference on Luminescence, Budapest, 1966* (Publishing House of the Hungarian Academy of Science, Budapest, 1966), p. 713.
[20] S. G. Zazubovich, N. E. Lushchik, and Ch. B. Lushchik, Izv. Akad. Nauk SSR **27**, 656 (1963).
[21] S. G. Zazubovich and T. A. Kuketaev, Tr. Inst. Fiz. i Astron. Akad. Nauk Est. SSR **31**, 190 (1966).
[22] R. Illingworth, Phys. Rev. **136**, A508 (1964).
[23] J. M. Donahue and K. Teegarden, J. Phys. Chem. Solids **29**, 2141 (1968).
[24] M. F. Trinkler, Opt. i Spektroskopiya **18**, 884 (1965) [Opt. Spectry. (USSR) **18**, 495 (1965)].
[25] M. F. Trinkler and I. K. Plyavin, Phys. Status Solidi **11**, 277 (1965).
[26] N. N. Kristoffel, in Ref. 19, p. 824.

rather meager. Most of the data were obtained at temperatures above the boiling point of liquid nitrogen[7,19–21,27]; from experience with Tl^+, data at various temperatures are expected to be quite complex, interesting, and useful. We report here rather systematic emission data on Ga^+ and In^+ in KI, KBr, KCl, and NaCl and also preliminary data on Sn^{2+} in KI and KBr. It will become clear that emission spectra excitable in the A-absorption band of Ga^+ and In^+ are quite similar to those of Tl^+.

The sample crystals were obtained by the method described previously[12–14] and their dimensions were about $8\times8\times2$ mm^3. The concentration of impurity ions was 10^{17}–10^{18}/cm^3. The sample was mounted on an aluminum holder which was immersed in liquid helium contained in a $(20\times20\times30)$-mm^3 fused silica cell. The cell was connected with a graded seal to the liquid-helium vessel made of glass. The temperature was controlled by the use of a heater attached to the aluminum holder after the liquid helium had completely evaporated. The temperature was measured with Au(Co)-Cu thermocouple and was maintained within $\pm1\%$ during a particular measurement of emission spectra. The sample was irradiated with a Ushio 500-W Xe lamp through a Karl-Leiss prism double monochromator. Emission spectra were obtained at right angles to the exciting light by the use of a Perkin-Elmer double-pass monochromator model 122 and an EMI 6256S photomultiplier. The bandpass of the exciting and detecting monochromator is about 30 and 60 meV, respectively. The combination of the entrance lens, the monochromator, and the photomultiplier was calibrated using a National Bureau of Standards standard lamp. The calibration was made accurately in the wavelength range shorter than 550 nm. The accuracy grows poor as the wavelength becomes longer, because the sensitivity of the photomultiplier decreases rapidly. Hence, the detailed shape of the low-energy part of the emission spectra is obscured.

In Fig. 1 are shown the emission spectra of Ga^+ and In^+ excitable in the A-absorption band at various temperatures. The emission spectra are presented by assuming that the quantum yield does not change as the temperature changes, i.e., the total area under the emission bands are suitably normalized. In Fig. 2 are shown the emission spectra of Sn^{2+} at 4.2°K. Two emission bands are observed; both of the emission bands appear with comparable intensity when excited in the high-energy part of the A-absorption band, while the high-energy emission mainly appears when excited in the high-energy part. It is clear from Figs. 1 and 2 that the phosphors are divided into four groups as shown in Table II according to the type of temperature variations of the emission spectra.

The temperature variation of the group (1) is rather complex and interesting. At 4.2°K the high-energy emission band (hereafter designated as A_T) mainly appears and the intensity of the low-energy emission band (hereafter designated as A_X) is several percent of the A_T emission band. Up to about 40°K no drastic change occurs. Between about 40 and 80°K the A_T emission band decreases while the A_X emission band increases, and at least between about 80–140°K the A_X emission band is the main result of excitation in the A-absorption band. The emission spectra above about 140°K consist of a broad band with a high-energy tail or shoulder, which is remarkably clear in the case of NaCl:Ga and KI:In. The peak of the broad band becomes separated from that of the A_X emission band toward high-energy side with the rise of temperature.

TABLE II. KI:Tl-type phosphors are divided into four groups according to the characteristic temperature variations of the emission spectra excited in the A-absorption bands shown in Figs. 1 and 2. The temperature variation of the group (2) is nearly same as that of the group (1), except that there is no temperature region in which the A_X emission band is mainly observed. The temperature variation of the group (3) is quite simple. In the case of the group (4) phosphors two emission bands appear with comparable intensity when excited in the high-energy part of the A-absorption band even at 4.2°K.

Group	Phosphors
(1)	KI:Ga, KBr:Ga, KCl:Ga, NaCl:Ga, KI:In, KI:Tl
(2)	KBr:In, KBr:Tl
(3)	KCl:In, NaCl:In, KCl:Tl
(4)	KI:Sn, KBr:Sn, KCl:Sn

The temperature variation of the group (2) is nearly the same as that of the group (1), except that there is no temperature region in which the A_X emission band is mainly observed. The temperature variation of the group (3) is quite simple. There is only one emission band in the temperature region from 4.2 to 300°K. The emission band broadens and shifts slightly as the temperature increases. Since the temperature variation of the group (1) and (2) is quite similar to one another there must exist a general explanation for the characteristic tempeature variations. The explanation is the JTE together with the spin-orbit interaction, i.e., the existence of two kinds of minima on the $\Gamma_4^-(^3T_{1u})$ APES, as will be made clear in the later sections. It is also likely, though not clear in the present investigation, that the characteristic features of the group (4) are explained in terms of the JTE and the spin-orbit interaction.

III. WHY A_X EMISSION COULD NOT BE ASSIGNED TO INVERSE PROCESS OF D-ABSORPTION BAND

Before presenting detailed explanations based on the JTE, we shall point out in this section difficulties concerning the explanation (d) of Table I. The following four facts seem to indicate why the A_X emission could not be assigned to the destruction of an exciton perturbed by an adjacent impurity ion (Ga^+, In^+, or Tl^+), i.e., to the inverse process of the D absorption.

[27] S. G. Zazubovich, Opt. i Spektroskopiya 26, 235 (1969) [Opt. Spectry. (USSR) 26, 126 (1969)].

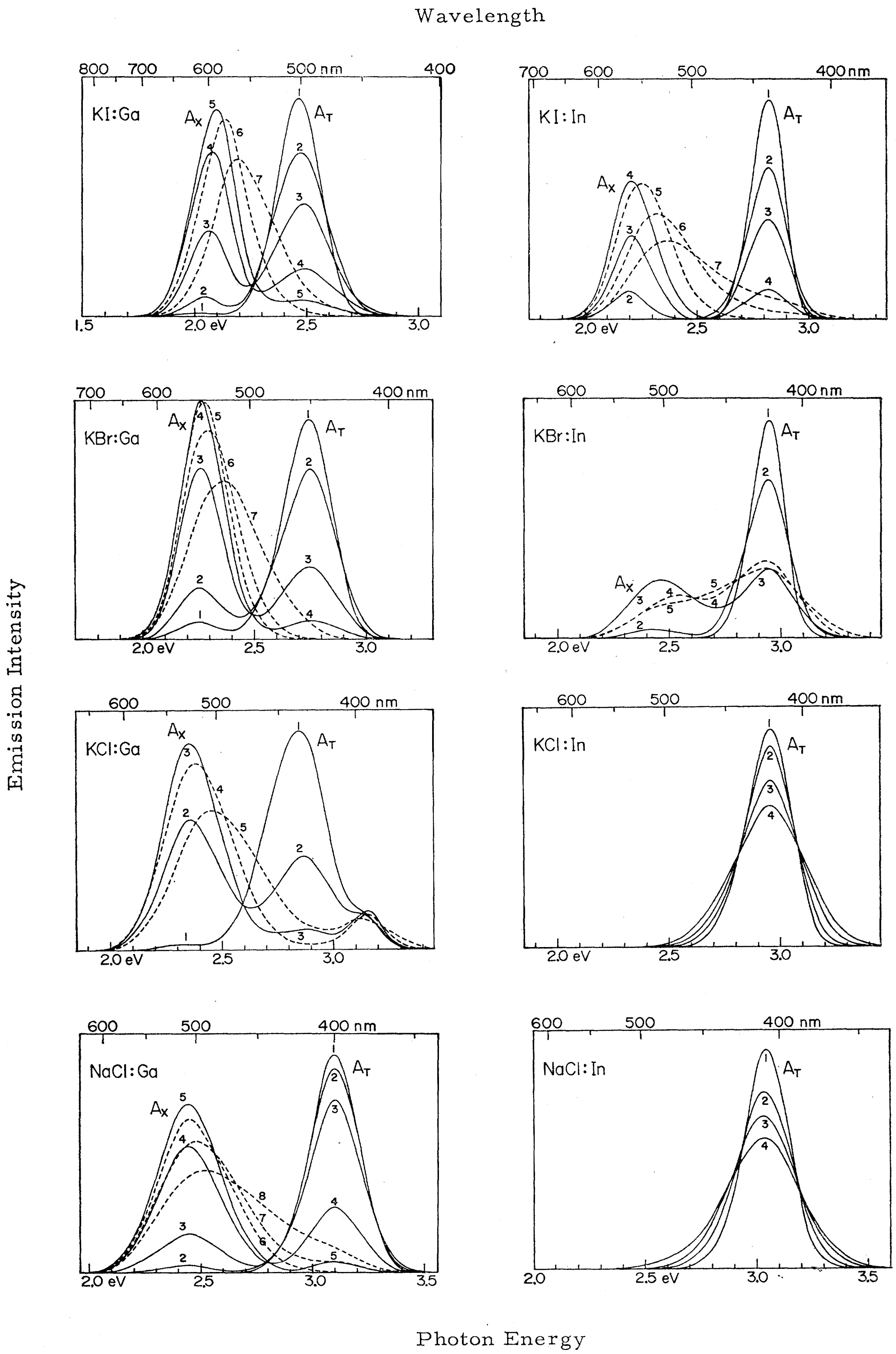
Wavelength
Emission Intensity
Photon Energy
KI:Ga
KI:In
KBr:Ga
KBr:In
KCl:Ga
KCl:In
NaCl:Ga
NaCl:In
A_X
A_T
800 700 600 500 nm 400
700 600 500 400 nm
1.5 2.0 eV 2.5 3.0
2.0 eV 2.5 3.0
600 500 400 nm
2.0 eV 2.5 3.0 3.5
2.0 2.5 eV 3.0 3.5

FIG. 1.

TABLE III. Ratio in intensity between the A_X and A_T emission bands, A_X/A_T, at 4.2°K when excited in the A-, C-, and D-absorption bands.

	A	C	D	References
KI:Ga	~0.09	0.6	0.4	
KI:In	~0.02	0.3	0.3	
NaI:Tl			0.2	17
KI:Tl	~0.01		1.8	23(20°K)
KBr:Tl	~0.01		4.9	23(20°K)

(i) The only reliable basis on which Illingworth[22] and Donahue and Teegarden[23] suggest explanation (d) is the fact that the A_X emission is stimulated most efficiently in the D-absorption band in case of KI:Tl and KBr:Tl. In order to check this basis, emission spectra in KI:Ga and KI:In were obtained at 4.2°K by exciting in the A-, C-, and D-absorption bands, with special attention being paid to the ratio in intensity between the A_X and A_T emission bands. We used the same monochromators mentioned in Sec. II. As a light source and a detector, a Hitachi hydrogen lamp and a HTV R-136 photomultiplier were used. Since the photomultiplier is sensitive up to 800 nm, the calibration was made accurately in the wavelength range shorter than 650 nm. The results are summarized in Table III together with those obtained by Fontana *et al.*[17] and also by Donahue and Teegarden.[23] It should be noted that, in case of NaI:Tl and KI:In, even the D-band excitation does not result in the prominent A_X emission, and that, in case of KI:Ga, the C absorption stimulates the A_X emission more efficiently than the D absorption does.

(ii) If the A_X emission is due to the destruction of an exciton perturbed by an adjacent impurity ion (Ga^+, In^+, or Tl^+), the radiative lifetime of the perturbed exciton would not strongly depend on the impurity ion. Illingworth[22] measured the decay time of the A_X emission in KI:Tl and KBr:Tl and concluded that the radiative lifetime of the perturbed exciton is less than 5×10^{-8} sec. We measured the decay time of the A_X emission in KI:Ga and KI:In at various temperatures from 50 to 273°K. To measure the decay time,[28] a pulse of light from a spark source was passed through the Ferié prism monochromator and focused on a sample. Pulses of duration 1×10^{-8} and 1×10^{-7} were formed with air gaps. The light emitted by the sample at right angles to the exciting light passed through a filter and was detected with a selected HTV R-136 photomulti-

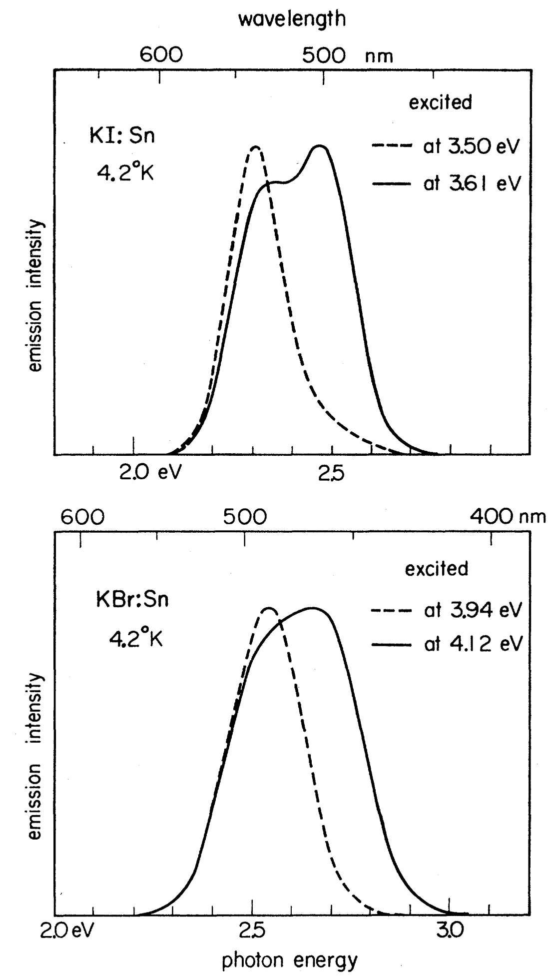

FIG. 2. Emission spectra at 4.2°K excitable in the A-absorption band of Sn^{2+} in KI and KBr. Two emission bands appear with comparable intensity even at 4.2°K. Excitation spectra for each emission are completely different from each other even within the A-absorption band; the high-energy emission appears only when excited in the high-energy part of the A-absorption band.

FIG. 1. Emission spectra at various temperatures excited in the A-absorption band of Ga^+ and In^+ in several alkali halides. The emission spectra are presented by assuming that the quantum yield does not change as the temperature changes, i.e., the total area under the emission bands are suitably normalized. The emission band at 3.15 eV in KCl:Ga is due to Pb^{2+} impurity ions the sample (accidentally) contained. Temperatures (°K) are as follows:

	1	2	3	4	5	6	7	8
KI:Ga	4.2	50	56	64	76	138	273	
KBr:Ga	4.2	44	51	57	77	190	273	
KCl:Ga	4.2	40	46	131	275			
NaCl:Ga	4.2	45	51	58	66	131	180	278
KI:In	4.2	57	72	79	131	226	296	
KBr:In	4.2	77	131	180	275			
KCl:In	4.2	77	144	203				
NaCl:In	4.2	131	203	273				

[28] The author is indebted to S. Yano at the Institute for Optical Research, Kyoiku University for decay-time measurements.

TABLE IV. Radiative lifetime of the excited state responsible for the A_X emission.

	τ_{rad}	References
KI:Ga	9×10^{-6}	
KI:In	3×10^{-6}	
KI:Tl	Less than 5×10^{-8}	22
KBr:Tl	Less than 5×10^{-8}	22

plier. The photocurrent was displayed on an Textronix synchroscope model 545. The synchroscope traces of single pulses were photographed. The rise time of the detecting system was less than 1×10^{-8} sec. The results are summarized in Table IV. It should be noted that the decay time of the A_X emission in KI:Ga and KI:In is simple, temperature independent, and two orders of magnitude as long as that of the fast component of the A_X emission in KI:Tl.

(iii) The perturbed exciton is most likely trapped in the form of a V_K center plus an electron immediately adjacent to an impurity ion (Ga^+, In^+, or Tl^+).[23] Hence the A_X emission would be the recombination luminescence of (V_K+electron) adjacent to an impurity ion, which was found in KCl:Tl and KI:Tl in the afterglow of x or γ irradiation. The recombination luminescence appears at 425 nm in KI:Tl[29] and 410 nm in KCl:Tl.[30] It should be noted that, in the case of KCl:Tl, the A- and D-band excitation does not result in the 410-nm emission band. In the case of KI:Tl, although both of the recombination luminescence and the A_X emission appear near at 425 nm, the former is broader than the latter. Moreover, our preliminary experiment of afterglow following x irradiation of KBr:Tl shows that the A_X emission peaking at near 355 nm could not be found in the afterglow. In this way, it is safe to conclude that the A_X emission is not the recombination luminescence, and hence is not due to the inverse process of the D absorption.

(iv) From the study of the structure of the A- and C-absorption bands[3–5,12–14] and the correlation of polarization between exciting and emitted light,[7,19] it has been firmly established that the JTE plays an important role in the $\Gamma_4^-(^1T_{1u}$ and $^3T_{1u})$ excited states. Moreover, the remarkable asymmetry of the A-band structure[3,5,12–14] and the temperature-dependent intensity of the A- and B-absorption bands[5] indicate the importance of the Jahn-Teller interaction between the spin-orbit split states Γ_1^-, Γ_4^-, Γ_3^-, and Γ_5^-. Then, according to Öpik and Pryce[8] and also to Kamimura and Sugano,[9] the Γ_4^- APES may have two kinds of minima. In this way, it is the most natural way to try to explain the observed emission spectra excitable in the A-absorption band in terms of the JTE and within the $a_{1g}t_{1u}$ electron configuration without introducing an additional level such as a perturbed exciton. In fact, it will become clear in Sec. V that several experimental results can be well explained along these lines.

IV. JTE IN $^3T_{1u}$ STATE: EXISTENCE OF TWO KINDS OF MINIMA ON $\Gamma_4^-(^3T_{1u})$ APES

The aim of this section is to give the minimum theoretical framework required to understand qualitatively the experimental results. This framework is essentially that discussed by Öpik and Pryce[8] and also by Kamimura and Sugano.[9] Hence the remainder of this section draws largely upon these papers. We shall consider the Jahn-Teller (electron-lattice) interaction in the linear approximation and within the $a_{1g}t_{1u}$ electron configuration. The lattice vibrational modes are represented by the six interaction-mode coordinates,[3] $Q_1(\alpha_{1g})$; Q_2 and $Q_3(\epsilon_g)$; Q_4, Q_5, and $Q_6(\tau_{2g})$, and the electron-lattice interaction is given by the matrix shown in Table V. For reference, the exchange and spin-orbit interaction matrix H_{so} is also given in Table VI. The problem is to diagonalize the matrix $H_{\mathrm{el}}+H_{\mathrm{so}}$ and to find minima of each APES by taking into account the lattice potential energy $\sum_{i=1}^{6} Q_i^2$. Optical transitions responsible for emission are considered to take place from these minima to the ground state at least at low temperatures. It is difficult, however, to solve the problem generally; in the following two assumptions will be used, Russell-Saunders coupling and the existence of tetragonal minima on the $\Gamma_4^-(^1T_{1u})$ APES, both of which have been experimentally verified to some extent.[7,12–14,31–33]

When the spin-orbit interaction is sufficiently small as compared with the exchange interaction $\zeta\ll G$, the off-diagonal matrix element between $^1T_{1u}$ and $^3T_{1u}$ may be neglected (Russell-Saunders coupling). Then $^1T_{1u}$ and $^3T_{1u}$ can be treated separately. In this approximation, Öpik and Pryce[8] positively showed that, on the $\Gamma_4^-(^1T_{1u})$ APES, there exists only one kind of minima which are tetragonal if and only if $b/c>1$ and trigonal if and only if $b/c<1$. The tetragonal minima exist in the $\epsilon_g(Q_2,Q_3)$ subspace and correspond to three distortions elongated or flattened along a [100], [010], or [001] direction. The trigonal minima, on the other hand, exist in the τ_{2g} (Q_4, Q_5, Q_6) subspace and correspond to four distortions elongated or flattened along a [111], [$\bar{1}$11], [1$\bar{1}$1], or [11$\bar{1}$] direction.[7]

It is difficult to know generally what kinds of minima there are on the Γ_5^-, Γ_3^-, Γ_4^-, $\Gamma_1^-(^3T_{1u})$ APES's. Since the experiments on the correlation of polarization[7,31–33] indicate that the $\Gamma_4^-(^3T_{1u})$ as well as the $\Gamma_4^-(^1T_{1u})$ APES's of Tl^+-type centers in several alkali halides have at least tetragonal minima, we shall try to find minima near the tetragonal configuration. To this end,

[29] W. B. Hadley, S. Polick, R. G. Kaufman, and H. N. Hersh, J. Chem. Phys. **45**, 2040 (1966).

[30] C. J. Delbecq, A. K. Ghosh, and P. H. Yuster, Phys. Rev. **151**, 599 (1966).

[31] C. C. Klick and D. W. Compton, J. Phys. Chem. Solids **7**, 170 (1958).

[32] R. Edgerton, Phys. Rev. **138**, A85 (1965).

[33] T. Shimada and M. Ishiguro, Phys. Rev. **187**, 1089 (1969); private communication.

TABLE V. The electron-lattice interaction matrix. Coupling constants with the α_{1g}, ϵ_g, and τ_{2g} modes are defined as follows:

$$a=\langle t_{1u,x}|\partial V/\partial Q_1|t_{1u,x}\rangle=\langle t_{1u,y}|\partial V/\partial Q_1|t_{1u,y}\rangle=\langle t_{1u,z}|\partial V/\partial Q_1|t_{1u,z}\rangle;$$
$$b=\langle t_{1u,x}|\partial V/\partial Q_2|t_{1u,x}\rangle=-\langle t_{1u,y}|\partial V/\partial Q_2|t_{1u,y}\rangle=-\sqrt{3}\langle t_{1u,x}|\partial V/\partial Q_3|t_{1u,x}\rangle=-\sqrt{3}\langle t_{1u,y}|\partial V/\partial Q_3|t_{1u,y}\rangle=\tfrac{1}{2}\sqrt{3}\langle t_{1u,z}|\partial V/\partial Q_3|t_{1u,z}\rangle;$$
$$c=\langle t_{1u,y}|\partial V/\partial Q_4|t_{1u,z}\rangle=\langle t_{1u,z}|\partial V/\partial Q_5|t_{1u,x}\rangle=\langle t_{1u,x}|\partial V/\partial Q_6|t_{1u,y}\rangle.$$

Basis functions are given at the left-handside of the matrix. Here $X_\pm$, etc., is symmetrized and antisymmetrized orbital wave functions given by $X_\pm=(1/\sqrt{2})\{a_{1g}(1)t_{1u,x}(2)\pm t_{1u,x}(1)a_{1g}(2)\}$, *etc.* and Θ_x, Θ_y, Θ_z, and Θ_0 are triplet and singlet spin functions given by $\Theta_x=-(1/\sqrt{2})\{\alpha(1)\alpha(2)-\beta(1)\beta(2)\}$, $\Theta_y=(i/\sqrt{2})\{\alpha(1)\alpha(2)+\beta(1)\beta(2)\}$, $\Theta_z=(1/\sqrt{2})\{\alpha(1)\beta(2)+\beta(1)\alpha(2)\}$, $\Theta_0=(1/\sqrt{2})\{\alpha(1)\beta(2)-\beta(1)\alpha(2)\}$.

				Γ_1^-	Γ_4^-			Γ_3^-		Γ_5^-			Γ_4		
		Γ_1^-	$\frac{1}{\sqrt{3}}(X_-\Theta_x+Y_-\Theta_y+Z_-\Theta_z)$	aQ_1		0		$\sqrt{\frac{2}{3}}bQ_2$	$\sqrt{\frac{2}{3}}bQ_3$	$\sqrt{\frac{2}{3}}cQ_4$	$\sqrt{\frac{2}{3}}cQ_5$	$\sqrt{\frac{2}{3}}cQ_6$		0	
			$\frac{i}{\sqrt{2}}(Z_-\Theta_y-Y_-\Theta_z)$		$aQ_1-\frac{b}{2}\left(Q_2-\frac{Q_3}{\sqrt{3}}\right)$	$-\frac{c}{2}Q_6$	$-\frac{c}{2}Q_5$	$-\frac{ic}{2}Q_4$	$-\frac{i\sqrt{3}c}{2}Q_4$	$\frac{ib}{2}(Q_2+\sqrt{3}Q_3)$	$-\frac{ic}{2}Q_6$	$\frac{ic}{2}Q_5$			
	A	Γ_4^-	$\frac{i}{\sqrt{2}}(X_-\Theta_z-Z_-\Theta_x)$	0	$-\frac{c}{2}Q_6$	$aQ_1+\frac{b}{2}\left(Q_2+\frac{Q_3}{\sqrt{3}}\right)$	$-\frac{c}{2}Q_4$	$-\frac{ic}{2}Q_5$	$\frac{i\sqrt{3}c}{2}Q_5$	$\frac{ic}{2}Q_6$	$\frac{ib}{2}(Q_2-\sqrt{3}Q_3)$	$-\frac{ic}{2}Q_4$		0	
			$\frac{i}{\sqrt{2}}(Y_-\Theta_x-X_-\Theta_y)$		$-\frac{c}{2}Q_5$	$-\frac{c}{2}Q_4$	$aQ_1-\frac{b}{\sqrt{3}}Q_3$	icQ_6	0	$-\frac{ic}{2}Q_5$	$\frac{ic}{2}Q_4$	$-ibQ_2$			
$^3T_{1u}$		Γ_3^-	$\frac{1}{\sqrt{2}}(X_-\Theta_x-Y_-\Theta_y)$	0		0		$aQ_1-\frac{b}{\sqrt{3}}Q_3$	$-\frac{b}{\sqrt{3}}Q_2$	$-\frac{c}{2}Q_4$	$\frac{c}{2}Q_5$	0		0	
			$\frac{1}{\sqrt{6}}(2Z_-\Theta_z-X_-\Theta_x-Y_-\Theta_y)$						$aQ_1+\frac{b}{\sqrt{3}}Q_3$	$\frac{c}{2\sqrt{3}}Q_4$	$\frac{c}{2\sqrt{3}}Q_5$	$-\frac{c}{\sqrt{3}}Q_6$			
	B		$\frac{1}{\sqrt{2}}(Y_-\Theta_z+Z_-\Theta_y)$					$-\frac{c}{2}Q_4$	$\frac{c}{2\sqrt{3}}Q_4$	$aQ_1-\frac{b}{2}\left(Q_2-\frac{Q_3}{\sqrt{3}}\right)$	$\frac{c}{2}Q_6$	$\frac{c}{2}Q_5$			
		Γ_5^-	$\frac{1}{\sqrt{2}}(Z_-\Theta_x+X_-\Theta_z)$	0		0		$\frac{c}{2}Q_5$	$\frac{c}{2\sqrt{3}}Q_5$	$\frac{c}{2}Q_6$	$aQ_1+\frac{b}{2}\left(Q_2+\frac{Q_3}{\sqrt{3}}\right)$	$\frac{c}{2}Q_4$		0	
			$\frac{1}{\sqrt{2}}(X_-\Theta_y+Y_-\Theta_x)$					0	$-\frac{c}{\sqrt{3}}Q_6$	$\frac{c}{2}Q_5$	$\frac{c}{2}Q_4$	$aQ_1-\frac{b}{\sqrt{3}}Q_3$			
			$X_+\Theta_0$										$aQ_1+b\left(Q_2-\frac{Q_3}{\sqrt{3}}\right)$	cQ_6	cQ_5
$^1T_{1u}$	C	Γ_4^-	$Y_+\Theta_0$	0		0		0			0		cQ_6	$aQ_1-b\left(Q_2+\frac{Q_3}{\sqrt{3}}\right)$	cQ_4
			$Z_+\Theta_0$										cQ_5	cQ_4	$aQ_1+\frac{2b}{\sqrt{3}}Q_3$

TABLE VI. The exchange and spin-orbit interaction matrix.

			Γ_1^-	Γ_4^-	Γ_3^-	Γ_5^-	Γ_4^-
		Γ_1^-	$-G-\zeta$	0	0	0	0
${}^3T_{1u}$	A	Γ_4^-	0	$-G-\frac{1}{2}\zeta$	0	0	$(1/\sqrt{2})\zeta$
	B	Γ_3^-	0	0	$-G+\frac{1}{2}\zeta$	0	0
		Γ_5^-	0	0	0	$-G+\frac{1}{2}\zeta$	0
${}^1T_{1u}$	C	Γ_4^-	0	$(1/\sqrt{2})$	0	0	G

it is necessary to calculate the cross sections containing the Q_3 axis (purely tetragonal distortion), which is easily obtained as follows by diagonalizing $H_{\mathrm{el}}+H_{\mathrm{so}}$ for $Q_1=Q_2=Q_4=Q_5=Q_6=0$:

For

$$\Gamma_1^-(X_-\Theta_x+Y_-\Theta_y+Z_-\Theta_z),$$
$$\Gamma_3^-(2Z_-\Theta_z-X_-\Theta_x-Y_-\Theta_y),$$

we obtain

$$y=-x-\tfrac{1}{4}\mp(9x^2-\tfrac{3}{2}x+9/16)^{1/2};$$

for

$$\Gamma_4^-(Z_-\Theta_y-Y_-\Theta_z),\quad \Gamma_4^-(X_-\Theta_z-Z_-\Theta_x),$$
$$\Gamma_5^-(Y_-\Theta_z+Z_-\Theta_y),\quad \Gamma_5^-(Z_-\Theta_x+X_-\Theta_z),$$

we obtain

$$y=-x\mp(9x^2+\tfrac{1}{4})^{1/2}\quad\text{(doubly degenerate)};$$

for

$$\Gamma_4^-(Y_-\Theta_x-X_-\Theta_y),$$

we obtain

$$y=2x-\tfrac{1}{2};$$

and for

$$\Gamma_3^-(X_-\Theta_x-Y_-\Theta_y),\quad \Gamma_5^-(X_-\Theta_y+Y_-\Theta_x),$$

we obtain

$$y=2x+\tfrac{1}{2}\quad\text{(doubly degenerate)}.$$

This is shown in Fig. 3. For simplicity, the lattice potential energy is omitted. Solid lines mean nondegeneracy and dashed lines mean double degeneracy. Here

$$x=-\frac{b}{2\sqrt{3}\zeta}Q_3,\quad y=\frac{E'}{\zeta},\quad\text{and}\quad E'=E-\sum_{i=1}^{6}Q_i^2.$$

It should be noted that the cross sections containing the Q_3 axis are given uniquely if we use such dimensionless variables as x and y and neglect the lattice potential energy $\sum_{i=1}^6 Q_i^2$. As will be clear from Fig. 4,

$$b=\left\langle t_{1u,x}\left|\frac{\partial V}{\partial Q_2}\right|t_{1u,x}\right\rangle$$

may be negative if the t_{1u} orbital is well localized. In fact, the experiments with uniaxial stress made by Shimada and Ishiguro[33] showed that $b<0$ in KI:Tl.

We shall first consider the one extreme case that the spin-orbit interaction is small as compared with the electron-lattice interaction $\zeta\ll b^2$. In this case the ${}^3T_{1u}$ APES is approximated by the two asymptotes passing through the origin O, i.e.,

$$y=2x\qquad[E'/\zeta=(-b/\sqrt{3}\zeta)Q_3]$$

and

$$y=-4x\qquad[E'/\zeta=(2b/\sqrt{3}\zeta)Q_3].$$

This is nothing but the ${}^1T_{1u}$ APES (see Table V and

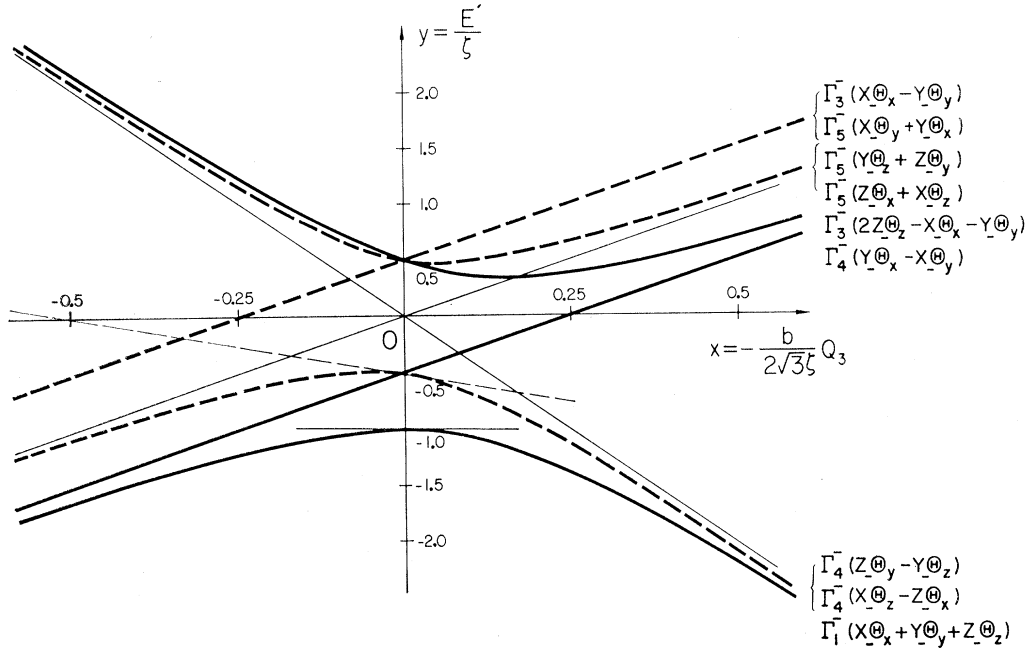

FIG. 3. Cross sections of the ${}^3T_{1u}$ APES containing the Q_3 axis (purely tetragonal distortion). For simplicity, the lattice potential energy is omitted. The abscissa is $x=-\frac{1}{2}\sqrt{3}bQ_3$ and the ordinate E'/ζ. Solid lines mean nondegeneracy and dashed lines double degeneracy.

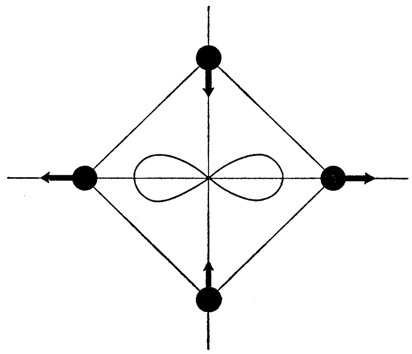

FIG. 4. The $t_{1u,x}$ MO and the Q_2 mode are shown schematically. This shows that $b=\langle t_{1u,x}|\partial V/\partial Q_2|t_{1u,x}\rangle$ may be negative if the $t_{1u,x}$ MO is well localized.

Fig. 5). Since the $\Gamma_4^-({}^1T_{1u})$ APES has tetragonal minima as mentioned above, the $\Gamma_4^-({}^3T_{1u})$ as well as the $\Gamma_1^-({}^3T_{1u})$ APES's must have minima near the tetragonal configuration up to a certain limiting value of ζ at which the minima disappear as ζ increases. Hereafter the tetragonal minima on the $\Gamma_1^-({}^3T_{1u})$ APES will be called eT minima. At the tetragonal configuration, however,

$$\Gamma_4^-(Z\_\Theta_y-Y\_\Theta_z) \quad \text{and} \quad \Gamma_4^-(X\_\Theta_z-Z\_\Theta_x),$$
$$\Gamma_4^-(X\_\Theta_z-Z\_\Theta_x) \quad \text{and} \quad \Gamma_4^-(Y\_\Theta_x-X\_\Theta_y),$$

and

$$\Gamma_4^-(Y\_\Theta_x-X\_\Theta_y) \quad \text{and} \quad \Gamma_4^-(Z\_\Theta_y-Y\_\Theta_z)$$

are degenerate so that the minima of the $\Gamma_4^-({}^3T_{1u})$ APES exist at configurations slightly lower than tetragonal. Hereafter, these six minima will be called X minima. In fact, Öpik and Pryce[8] positively showed by introducing the spin-orbit interaction as a perturbation that there are rhombic minima on the $\Gamma_4^-({}^3T_{1u})$ APES and tegragonal minima on the $\Gamma_1^-({}^3T_{1u})$ APES.

Next, we consider the other extreme case that the spin-orbit interaction is large as compared with the electron-lattice interaction but still small as compared with the exchange interaction $b^2 \ll \zeta \ll G$. In this case the ${}^3T_{1u}$ APES shown in Fig. 3 can be approximated by

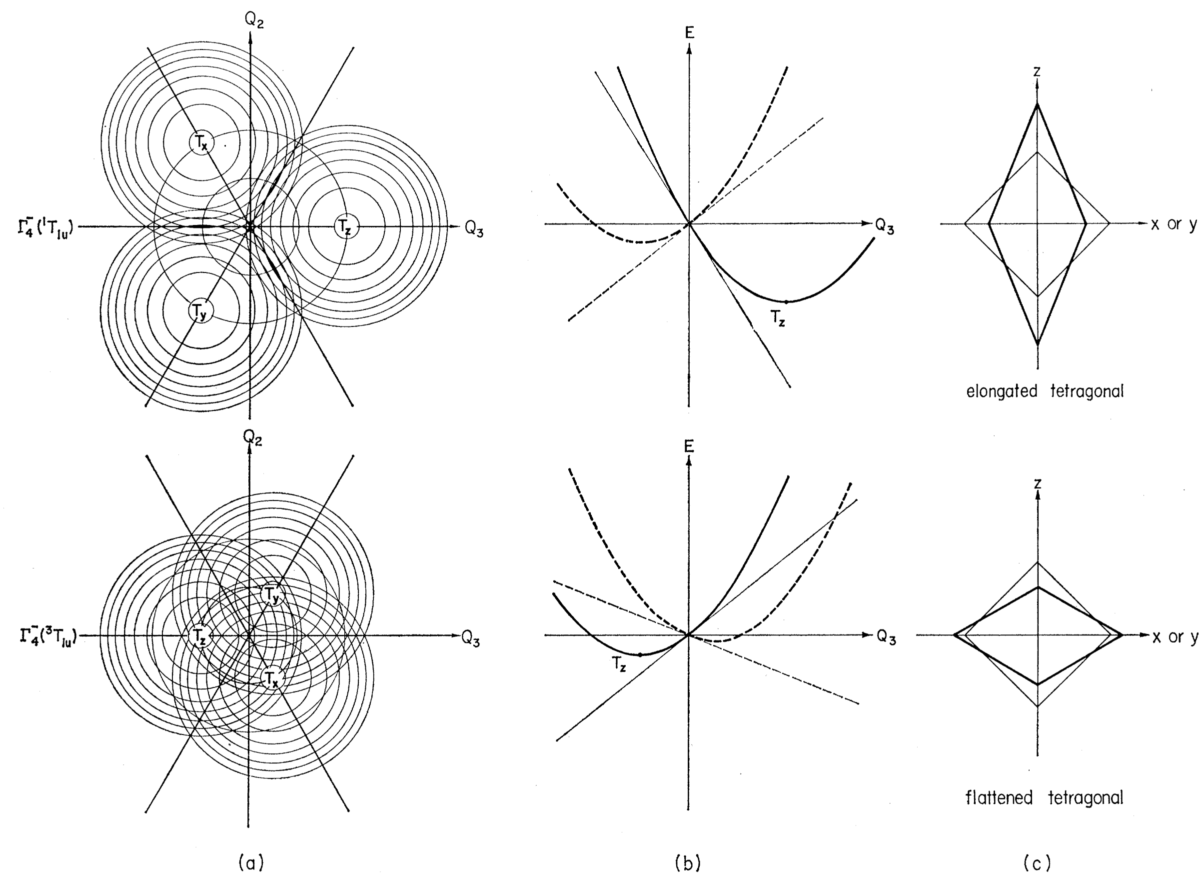

FIG. 5. (a) The $\Gamma_4^-({}^1T_{1u})$ and $\Gamma_4^-({}^3T_{1u})$ APES's in the ϵ_g subspace which are obtained in the approximation that only the diagonal parts of $H_{so}+H_{el}$ are taken into account. Some of the contour lines are shown. Minima on the $\Gamma_4^-({}^1T_{1u})$ APES are situated at $(q,0)$, $(-\frac{1}{2}q, \frac{1}{2}\sqrt{3}q)$ and $(-\frac{1}{2}q, -\frac{1}{2}\sqrt{3}q)$, while those on the $\Gamma_4^-({}^3T_{1u})$ APES at $(-\frac{1}{2}q, 0)$, $(\frac{1}{4}q, -\frac{1}{4}\sqrt{3}q)$, and $(\frac{1}{4}q, \frac{1}{4}\sqrt{3}q)$. (b) Parabolas show the cross sections of the Γ_4^- APES's containing the Q_3 axis. When the lattice potential energy is omitted, parabolas become straight lines. Solid lines mean nondegeneracy and dotted ones double degeneracy. The minima on the $\Gamma_4^-({}^1T_{1u})$ APES is four times deeper than that of the $\Gamma_4^-({}^3T_{1u})$ APES. (c) The corresponding distortions around the center are schematically shown.

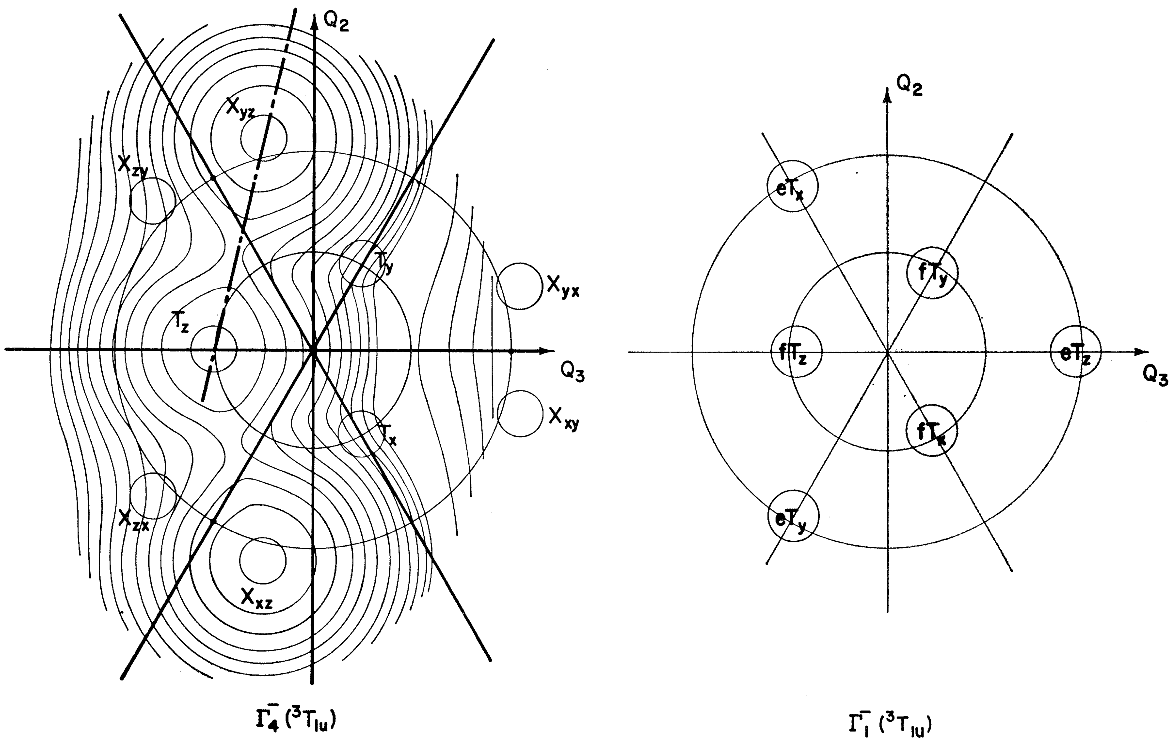

FIG. 6. Minima on the $\Gamma_4^-({}^3T_{1u})$ and $\Gamma_1^-({}^3T_{1u})$ APES are schematically drawn. There are two kinds of minima on both of the APES's. Contour lines of the $\Gamma_4^-(Y_-\Theta_x - X_-\Theta_y)$ sheet are also schematically shown.

tangents at $Q_3=0$. This approximation corresponds to that of considering only the diagonal parts of the electron-lattice interaction matrix shown in Table V. As is clear in this matrix, the diagonal part for $\Gamma_4^-({}^3T_{1u})$ is of the same form as that for $\Gamma_4^-({}^1T_{1u})$, except the value of the electron-lattice interaction parameters; the parameters are a, $-\frac{1}{2}b$ and $-\frac{1}{2}c$ in the $\Gamma_4^-({}^3T_{1u})$ state and a, b, and c in the $\Gamma_4^-({}^1T_{1u})$ state. Therefore, when the $\Gamma_4^-({}^1T_{1u})$ APES has a minimum at $Q_3=q$, the $\Gamma_4^-({}^3T_{1u})$ APES also has a minimum at $Q_3=-\frac{1}{2}q$. This is to be the case up to a certain limiting value of ζ at which the minimum disappears as ζ decreases, because the cross section of the $\Gamma_4^-(Y_-\Theta_x - X_-\Theta_y)$ APES is given by a straight line as shown in Fig. 3. There exist two other corresponding minima on the $\Gamma_4^-(Z_-\Theta_y - Y_-\Theta_z)$ and $\Gamma_4^-(X_-\Theta_z - Z_-\Theta_x)$ APES's. Hereafter these tetragonal minima will be designated as T minima. In Fig. 5 are shown the $\Gamma_4^-({}^1T_{1u})$ and $\Gamma_4^-({}^3T_{1u})$ APES's in this approximation. Since the diagonal part for $\Gamma_1^-({}^3T_{1u})$ in Table V does not depend on Q_i other than Q_1, the tangent of the $\Gamma_1^-({}^3T_{1u})$ APES is given by a straight line parallel to the Q_3 axis. Therefore, if the spin-orbit interaction is so large that the $\Gamma_1^-({}^3T_{1u})$ APES shown in Fig. 3 can be approximated by its tangent at $Q_3=0$, there exists only one totally symmetric minimum on the $\Gamma_1^-({}^3T_{1u})$ APES. When the interaction is suitably large, however, the $\Gamma_1^-({}^3T_{1u})$ APES may also have three tetragonal minima which correspond to T minima on the $\Gamma_4^-({}^3T_{1u})$ APES. Hereafter, these tetragonal minima will be designated as fT minima.

In this way it becomes clear that, when the spin-orbit interaction is of suitable value as compared with the electron-lattice interaction, there may exist two kinds of minima, T and X, on the $\Gamma_4^-({}^3T_{1u})$ APES and also two kinds of minima, fT and eT, on the $\Gamma_1^-({}^3T_{1u})$ APES. These minima are schematically shown in Fig. 6. Let us examine a little more quantitatively how these minima vary with the spin-orbit and electron-lattice interaction parameters, ζ and b^2. To this end, we shall consider the cross sections of the $\Gamma_4^-({}^3T_{1u})$ and $\Gamma_1^-({}^3T_{1u})$ APES's containing the Q_3 axis without neglecting the lattice potential energy. It should be noted that the lattice potential energy is given by

$$\frac{E-E'}{\zeta} = \frac{(1-\beta)}{\zeta} Q_3^2 = \frac{12\zeta(1-\beta)}{b^2} x^2,$$

where β is the difference in curvature between the excited and the ground APES's, which is a part of quadratic interactions.[5,34,35] Inclusion of $(1-\beta)$ in the lattice potential energy is necessary, because the analysis of the absorption band clearly indicates that the curvature of the excited APES is remarkably smaller than that of the ground APES.[5,34] Thus the

[34] A. Honma, Sci. Light (Japan) 17, 34 (1968); 18, 33 (1969).

[35] It should be noted that, in the linear interaction, the lattice potential energy is always given by $\sum_{i=1}^{6} Q_i^2$ when use is made of the interaction-mode coordinates.

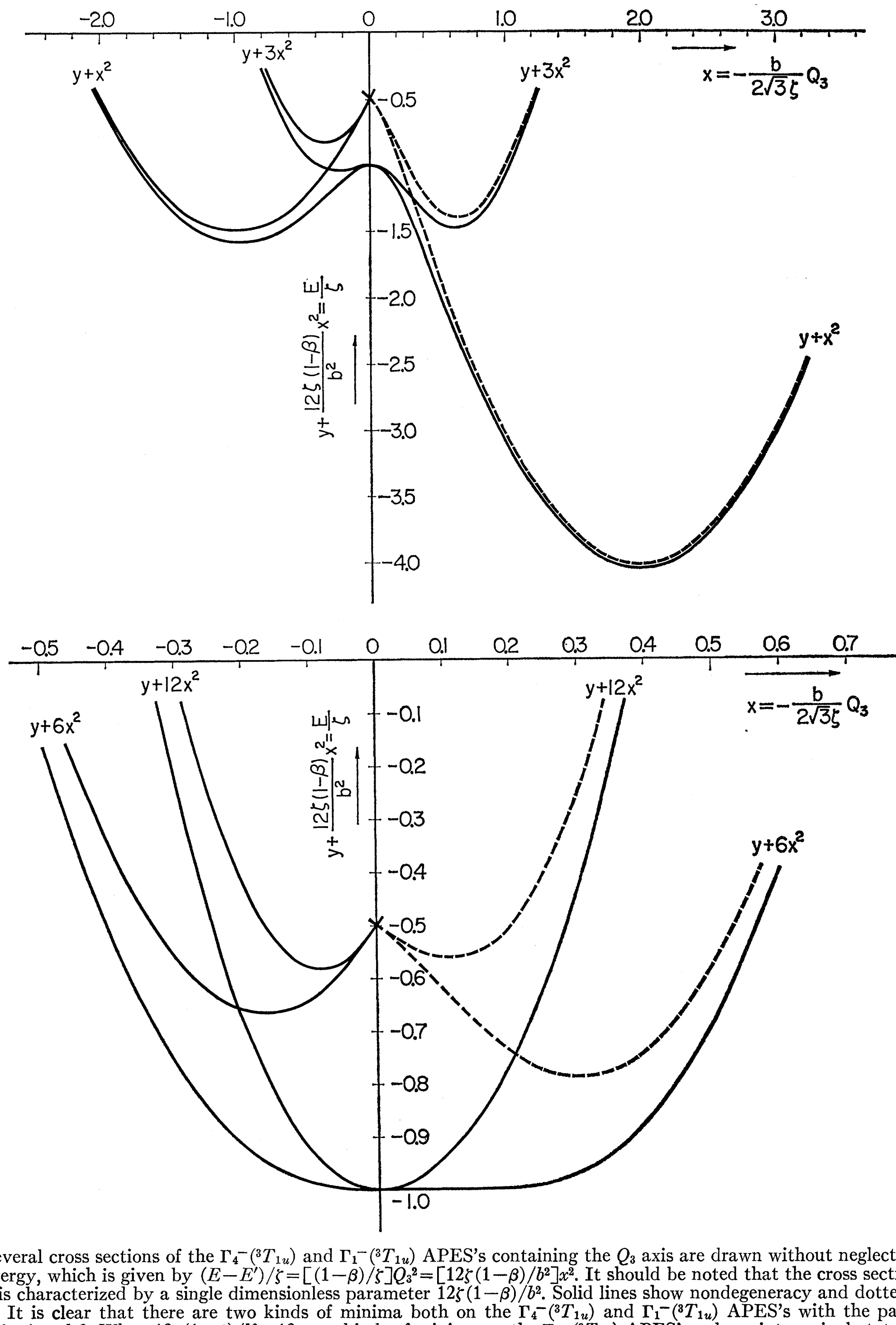

FIG. 7. Several cross sections of the $\Gamma_4^-({}^3T_{1u})$ and $\Gamma_1^-({}^3T_{1u})$ APES's containing the Q_3 axis are drawn without neglecting the lattice potential energy, which is given by $(E-E')/\zeta=[(1-\beta)/\zeta]Q_3^2=[12\zeta(1-\beta)/b^2]x^2$. It should be noted that the cross section containing the Q_3 axis is characterized by a single dimensionless parameter $12\zeta(1-\beta)/b^2$. Solid lines show nondegeneracy and dotted lines double degeneracy. It is clear that there are two kinds of minima both on the $\Gamma_4^-({}^3T_{1u})$ and $\Gamma_1^-({}^3T_{1u})$ APES's with the parameter value $12\zeta(1-\beta)/b^2=1$ and 3. When $12\zeta(1-\beta)/b^2=12$, two kinds of minima on the $\Gamma_1^-({}^3T_{1u})$ APES' coalesce into a single totally symmetric minimum and, at the same time, the minimum on the dotted curve becomes shallower than the minimum on the solid curve which is one of the T minima. In such a situation, there may exist no X minima [see Fig. 5(b)].

cross section containing Q_3 axis is characterized by a single dimenionless parameter $12\zeta(1-\beta)/b^2$. In Fig. 7 are given various cross sections with different parameter values. Figure 7 indicates that the relative depths of the X and T minima vary with the value of $12\zeta(1-\beta)/b^2$. Although it is difficult to determine the values of ζ, β, and b^2 accurately, a rough estimate of these values, is as follows: $\zeta=0.1\sim0.7$ eV,[12–14] $b^2=0.8\sim3$ eV,[3] and

TABLE VII. Summary of the observed emission peaks at 4.2°K and their assignments.

	A_X (eV)	A_T (eV)	References
KI:Ga	2.04	2.47	
KBr:Ga	2.24	2.74	
KCl:Ga	2.35	2.85	
NaCl:Ga	2.45	3.10	
KI:In	2.20	2.81	
KBr:In	2.46	2.94	
KCl:In	···	2.95	
NaCl:In	···	3.05	
NaI:Tl	2.88	3.75	17
KI:Tl	2.89	3.70	23 (20°K)
KBr:Tl	3.50	4.02	23 (20°K)
RbBr:Tl	3.28	3.90	18 (77°K)
KCl:Tl	···	4.17	23 (20°K)
RbCl.:Tl	3.53	3.95	18 (77°K)

$\beta=0.1\sim0.6$.[34] When $12\zeta(1-\beta)/b^2$ is as small as 1, the X minima are considerably deeper than the T minima, and the fT and eT minima are close to the T and X minima, respectively. Three typical cases are distinguished according to the relative depths of the T and X minima. (1) The depth of the X minima are considerably deeper than that of the T minima. (2) The depth of the X minima is nearly equal to that of the T minima. (3) There exist no X minima. Group (1) contains phosphors which are expected to have smaller $12\zeta(1-\beta)/b^2$ values, while group (3) contains phosphors which are expected to have larger $12\zeta(1-\beta)/b^2$ values, i.e., Ga^+ has a smaller ζ value than In^+ [12–14] and KI has a larger β value than KCl.[5,34] Therefore, it is reasonable to correlate these three cases to the three groups and to consider that the A_T and A_X emission bands are due to the transitions from the T and X minima to the ground state, respectively. Thus, we can explain in Sec. V several observed features concerning the emission excitable in the A absorption.

There is one difficulty; in case (2) and especially in case (3), Fig. 7 indicates that the fT and eT minima coalesce into the totally symmetric minimum. Therefore, it is difficult to explain the polarization of the slow component of the A_T emission as will be mentioned in Sec. V C.[36] The difficulty may result from the several assumptions used: (1) At least in case of Tl^+, the breakdown of the Russel-Saunders coupling is crucial. (2) Higher-order interactions are neglected other than the difference in the force constants which is a part of the quadratic interactions. (3) The anharmonicity is also neglected. (4) The electron-lattice interaction is treated in the $\epsilon_g(Q_2,Q_3)$ subspace. (5) The electron-lattice interaction is treated in the $a_{1g}t_{1u}$ manifold. (6) The MO's a_{1g} and t_{1u} themselves are assumed not to change during relaxation. Unfortunately, we could not decide at present which approximation is essential for the difficulty.

[36] Gebhardt *et al.* also tried to explain the polarization of the slow component of the A emission in KCl by assuming nontotally symmetric minima on the $\Gamma_1^-({}^3T_{1u})$ APES. But they did not solve the difficulty, either. [Report at the International Conference on Luminescence, Delaware, 1969 (to be published).]

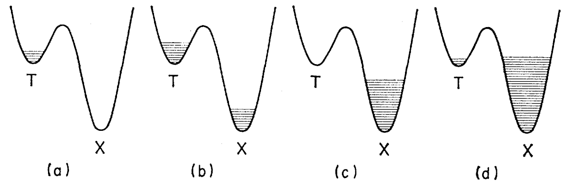

FIG. 8. Curves schematically show the cross section of the $\Gamma_4^-({}^3T_{1u})$ APES along the dotted line in Fig. 6. Hatches show the distribution of the system. (a) At very low temperatures the T minima are preferentially populated by the mechanism mentioned in the text. The barrier between the T and X minima is so high that only a small part of the system arrives at the X minima. (b) As the temperature is raised, part of the system arrives at the X minima. (c) As the temperature is raised still higher, most of the system arrives at the X minima. (d) At very high temperatures, both minima are populated. These variations of the distribution can explain the temperature variation of the emission spectra shown in Fig. 1.

V. TO WHAT EXTENT CAN JTE EXPLAIN OBSERVED FEATURES?

Now let us explain several observed features concerning the luminescence excitable in the A-absorption band. To this end, we adopt the assignments shown in Table VII. Note that the A_T and A_X emission bands are considered to be due to the transition from the T and X minima to the ground state, respectively, and that, in case of phosphors belonging to group (3), no A_X emission is considered to appear. A few authors supposed that, in the case of KCl:Tl, the two emission bands overlap each other.[16,22,25] In fact, by the use of time-resolved spectroscopy, Trinkler *et al.*[37] positively confirmed that the peak of the "slow component" is slightly shifted toward low energy as compared with that of the "fast component." Therefore, the A_T and A_X emission may accidentally overlap each other. There exists, however, another possibility that the emission $\Gamma_1^-({}^3T_{1u})\rightarrow\Gamma_1^+({}^1A_{1g})$ may be observed (see Sec. V C). For the present, the author adopted the latter possibility and hence the assignment shown in Table VII.

A. Emission Spectra

According to the discussion in Sec. IV, the existence of the three groups is ascribed to the existence of the three cases. The characteristic temperature variation of the emission spectra excitable in the A absorption are qualitatively explained in terms of the distribution of the system over the T and X minima. We consider case (1), i.e., group (1) phosphors, as a typical example. The distribution varies with temperature as shown in Fig. 8.

[37] M. F. Trinkler, I. K. Plyavin, B. Ya. Berzin, and A. K. Everte, Opt. i Spektroskopiya **19**, 373 (1965) [Opt. Spectry. (USSR) **19**, 213 (1965)].

(a) When the temperature is sufficiently low as compared with the barrier between the T and X minima, i.e., below about 40°K, the A_T emission band appears preferentially because the T minima are mainly populated in the "cooling" process as will be described in Sec. V B. Moreover, the shape of the A_T emission band shows no remarkable change, because at such low temperatures the thermal distribution of the system is mainly determined by the zero-point vibrations around the T minima and scarcely depends on temperature.

(b) The abrupt change observed between about 40 and 80°K is mainly caused by the probability that the system once relaxed to the T minima may thermally go from the T minima to the X minima. The probability increases markedly with the rise of temperature. At such low temperatures, however, the radiative transitions may occur before most of the system arrives at the X minima. Hence both of the A_T and A_X emission bands appear and the ratio in intensity A_X/A_T increases with the rise of temperature.

(c) In the temperature range between about 80 and 140°K, the probability becomes so large that most of the system arrives at the X minima before the radiative transitions occur. Hence the A_X emission band appears predominantly. The asymmetry deformed toward the high-energy side may be due to the fact that the APES could no longer be approximated by paraboloid in this temperature range.

(d) Above 140°K thermal equilibrium is established between the T and X minima. Hence both of the A_T and A_X emission bands appear as is clearly seen in NaCl:Ga and KI:In. The distribution, however, is not restricted to the bottom of the minima, so that the emission spectra could not be reproduced by adding the suitably weighted A_T and AX emission bands at low temperatures.

In case (2), the depth of the X minima is nearly equal to that of the T minima. Hence there is no temperature range in which the A_X emission predominantly appears. It should be noted that the X minima are further separated from the origin than the T minima. For this reason, the A_X emission always appears in the lower energy than the A_T emission, even when the depth of the X minima is nearly equal to that of the T minima. Case (3) is so simple that no explanation is necessary.

B. Excitation Spectra for A_T and A_X Emission Bands

Three characteristic features observed at low temperatures will be explained:

(1) The A_T emission is preferentially excited in the A-absorption band. This feature was found in KI:Tl and KBr:Tl by Edgerton and Teegarden,[16] and in NaI:Tl by Fontana *et al.*,[17] and was confirmed rather systematically in Fig. 1.

(2) The excitation spectrum for the A_X emission is slightly different from that for the A_T emission even

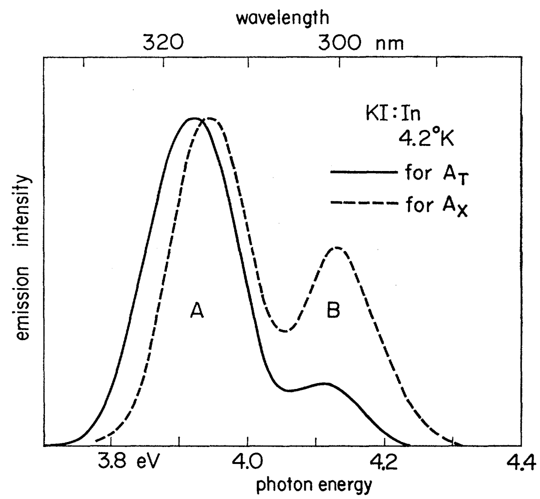

FIG. 9. Excitation spectra for the A_T and A_X emission. Peaks are normalized.

in the region of the A-absorption band; the A_X emission is excited more efficiently on the high-energy side of the A-absorption band than on its low-energy side. This feature was found in KI:Tl by Trinkler and Plyavin[24,25] and was confirmed, in the present study, rather systematically in KI:Ga, KBr:Ga, KCl:Ga, KI:In, and KBr:In. An example is given in Fig. 9.

(3) Excitation in the B-, C-, or D-absorption band produces rather strong A_X emission. As shown in Table III, the A_X emission becomes stronger than the A_T emission, when the excitation is made in the D-absorption band of KI:Tl and KBr:Tl.

We can explain these features schematically in the two-dimensional (ϵ_g) configuration coordinate space. Since the lattice vibrational motion is treated classically in the present approximation, the state of the system is characterized by a point (Q_2,Q_3) on the APES shown in Fig. 6. According to the Franck-Condon principle, the lattice configuration does not change during optical excitation. Hence the probability that the system arrives at a point (Q_2,Q_3) on the $\Gamma_4^-({}^3T_{1u})$ APES by the optical excitation is given by the thermal distribution on the ground $\Gamma_1^+({}^1A_{1g})$ APES,

$$(1/\pi kT)\exp[-(Q_3^2+Q_3^2)/kT].$$

Since the minima are so separated from the origin O that the distribution becomes practically zero near the T and X minima, the system could not arrive at the minima by the optical excitation alone. Relaxation after optical excitation is necessary for the population of the T and X minima. According to the general belief,[38] we envisage the relaxation as a process of sliding down the $\Gamma_4^-({}^3T_{1u})$ APES to its minima. Taking it into account that the sliding down may occur perpendicularly to the contour lines, we can easily understand

[38] D. L. Dexter and W. B. Fowler, J. Chem. Phys. **47**, 1379 (1967).

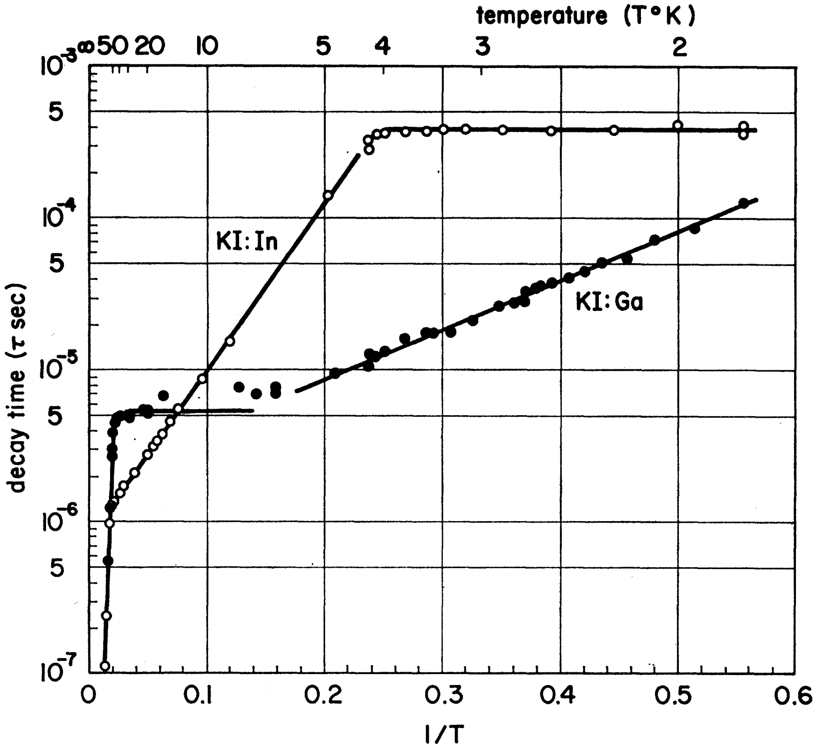

FIG. 10. Temperature variation of decay times of the A_T emission in KI:Ga and KI:In.

from Fig. 6(a) that the T minima is preferentially populated. Thus the A_T emission is preferentially excited in the A-absorption band.

Let us look at the $\Gamma_4^-(^3T_{1u})$ APES more in detail, paying special attention to the energy difference between the ground $\Gamma_1^+(^1A_{1g})$ and the excited $\Gamma_4^-(^3T_{1u})$ APES's, which corresponds to the photon energy of the exciting light. When the spin-orbit interaction is so large that the $\Gamma_4^-(^3T_{1u})$ APES is approximated by the tangent at the origin,[7] the energy difference is given by $E_0-(b/\sqrt{3})Q_3$, $(b<0)$. Even when the spin-orbit interaction is not so large that the $\Gamma_4^-(^3T_{1u})$ APES is complicated as shown in Fig. 6(a), it is possible to consider that the $Q_3>0$ region near the origin corresponds to the high-energy part of the A-absorption band and the $Q_3<0$ region to its low-energy part. As seen in Fig. 6(a), the system in the $Q_3>0$ region near the origin may relax to the X minima with larger probability than the system in the $Q_3<0$ region. Thus the A_X emission is excited more efficiently on the high-energy side of the A-absorption band than in its low-energy side.

It is difficult to obtain the probability that the system arrives at a point (Q_2,Q_3) on the $\Gamma_4^-(^3T_{1u})$ APES by the nonradiative transitions from the higher excited D, C, and B states. Roughly speaking, however, the probability may be large in the region where the APES's approaches one another. It is clear that the region is far separated from the origin. Hence the X minima may be populated more efficiently by the nonradiative transitions than by the optical excitation in the A absorption.

C. Decay Times

Various investigators[17,22,24,25,37,39,40] studied decay times of the A_T and A_X emission in case of Tl^+ and found that decay times are rather complex. Part of the emission (designated as a "fast component" by Illingworth[22]) is emitted within a short time of the order of 10^{-8} sec and the rest (designated as a "slow component") is emitted over a longer period with an exponential decay whose decay constant strongly depends on temperature. The relative proportion of the fast and slow components changes with temperature. The main results are as follows: (1) The decay time of the A_T emission at 10°K is simple and the order of 10^{-8} in case of KI:Tl and KBr:Tl. However, in case of KCl: Tl, it contains more than 80% slow component even at 10°K. (2) The decay time of A_X emission also contains fast and slow components in case of KI:Tl and KBr:Tl. Since there are no corresponding data in case of Ga^+ and In^+, decay times in KI:Ga and KI:In were obtained rather systematically in the present study. The decay times were measured by the same method described in Sec. III. Temperatures below 4.2°K were determined by the vapour pressure of

[39] I. K. Plyavin, B. Ya. Berzin, A. I. Niylisk, A. K. Tale, M. F. Trinkler, and V. G. Chernyak, in Ref. 19, p. 853.
[40] M. Tomura, T. Masuoka, and H. Nishimura, J. Phys. Soc. Japan 19, 1982 (1964).

helium. Main results are as follows: (3) The decay time of the A_T emission is complex and temperature dependent as shown in Fig. 10. Most of the A_T emission appears as a so-called slow component even at 4.2°K. (4) The decay time of the A_X emission above 77°K is simple as mentioned in Sec. III. Characteristic temperature variations of these decay times can be explained by introducing several radiative and nonradiative lifetimes τ as shown in Table VIII. Details will be explained in the following. It should be noted that nonradiative transitions may occur between particular minima shown in Fig. 6 at least at low temperatures.

$$T_z(\Gamma_4^-) \rightleftarrows fT_z(\Gamma_1^-), \quad \text{etc.},$$

$$T_z(\Gamma_4^-) \rightarrow \begin{cases} X_{yz}(\Gamma_4^-) \\ X_{xz}(\Gamma_4^-), \quad \text{etc.}, \end{cases}$$

$$fT_z(\Gamma_1^-) \rightarrow \begin{cases} eT_x(\Gamma_1^-) \\ eT_y(\Gamma_1^-), \quad \text{etc.}, \end{cases}$$

$$\left.\begin{matrix} X_{zx}(\Gamma_4^-) \\ X_{xz}(\Gamma_4^-) \end{matrix}\right\} \rightleftarrows eT_y(\Gamma_1^-), \quad \text{etc.}$$

We shall first consider the A_T emission at low temperatures. According to general belief, the first step is that the system is quasithermally distributed over the Γ_4^- APES near the T minima by the process of "sliding down."[38] When the radiative lifetime $\tau_{\text{rad}}[T(\Gamma_4^-) \rightarrow \Gamma_1^+]$ is long, part of the system makes nonradiative transition $T(\Gamma_4^-) \rightarrow fT(\Gamma_1^-)$. The relative proportions of the fast and slow components are determined by the relative values of $\tau_{\text{rad}}[T(\Gamma_4^-) \rightarrow \Gamma_1^+]$ and $\tau_{\text{nonrad}}[T(\Gamma_4^-) \rightarrow fT(\Gamma_1^-)]$ and hence are dependent on temperature.[22,25,38] When $\tau_{\text{rad}} < \tau_{\text{nonrad}}$, most of the A_T emission appears as the fast component, and vice versa. Since τ_{rad} may have the value of $\sim 5\times10^{-6}(\text{Ga}^+)$, $\sim 5\times10^{-7}(\text{In}^+)$, or $\sim 5\times10^{-8}(\text{Tl}^+)$, it is understandable that only the slow component is observed in KI:Ga, KI:In, and KCl:In, whereas only the fast component is observed in KBr:Tl and KI:Tl. It is difficult at present, however, to explain positively why the slow component of the A_T emission is not observed in KI:Tl and KBr:Tl and is observed in KCl:Tl.

Now we assume that most of the system arrives at the $fT(\Gamma_1^-)$ minima as in case of KI:Ga and KI:In. When $\tau_{\text{rad}}[T(\Gamma_4^-) \rightarrow \Gamma_1^+] \ll \tau_{\text{nonrad}}[fT(\Gamma_1^-) \rightarrow T(\Gamma_4^-)]$, τ_{nonrad} determines the decay time and the slow component of the A_T emission is observed.[22,41] When $\tau_{\text{rad}} \gg \tau_{\text{nonrad}}$, τ_{rad} determines the decay time. Figure 10 shows that, in case of KI:Ga, the decay time between 20 and 40°K is determined by $\tau_{\text{rad}} \sim 5\times10^{-6}$. Although the simple theory for nonradiative transitions may not be applicable for the nonradiative transition $fT(\Gamma_1^-) \rightarrow T(\Gamma_4^-)$, the so-called activation energies are obtained and summarized in Table IX because Fig. 10 indicates

[41] M. Tomura, H. Nishimura, Y. Kawashima, and K. Nishioka, Report at the Twenty-Third Annual Meeting of the Physical Society of Japan 5pL-6, Toyonaka, Osaka, 1968 (unpublished).

TABLE VIII. Summary of several radiative and nonradiative lifetimes (sec) responsible for decay times of the A_T and A_X emission. Since τ_{nonrad} depends strongly on temperature, temperatures (°K) are given in parentheses.

	A_T emission				A_X emission			
	τ_{rad} $[T(\Gamma_4^-) \rightarrow \Gamma_1^+]$	τ_{rad} $[fT(\Gamma_1^-) \rightarrow \Gamma_1^+]$	τ_{nonrad} $[fT(\Gamma_1^-) \rightarrow T(\Gamma_4^-)]$	τ_{nonrad} $[T(\Gamma_4^-) \rightarrow X(\Gamma_4^-)]$ $[fT(\Gamma_1^-) \rightarrow eT(\Gamma_1^-)]$	τ_{rad} $[X(\Gamma_4^-) \rightarrow \Gamma_1^+]$	τ_{rad} $[eT(\Gamma_1^-) \rightarrow \Gamma_1^+]$	τ_{nonrad} $[eT(\Gamma_1^-) \rightarrow X(\Gamma_4^-)]$	References
KI:Ga	5×10^{-6}	Longer than 10^{-4}	$9\times10^{-6}\sim1\times10^{-4}$ $(5\sim1.8)$	$10^{-8}\sim5\times10^{-6}$ $(100\sim40)$	9×10^{-6}			See Fig. 10
KI:In	Shorter than 10^{-6}	Longer than 4×10^{-4}	$1\times10^{-6}\sim4\times10^{-4}$ $(40\sim4)$	$10^{-8}\sim1\times10^{-6}$ $(100\sim40)$	3×10^{-6}			See Fig. 10
CsI:In				$10^{-8}(100)\sim$				39
KBr:In				$10^{-8}(100)\sim$				39
KCl:In			$3\times10^{-6}\sim1\times10^{-3}$ $(50\sim5)$					41
NaI:Tl	10^{-8}							17
KI:Tl	10^{-8}				10^{-8}	Longer than 3×10^{-3}	$10^{-7}\sim3\times10^{-3}$ $(300\sim50)$	22, 24, 25, 39
RbI:Tl	10^{-8}							39
KBr:Tl	10^{-8}				10^{-8}	Longer than 3×10^{-3}	$10^{-7}\sim3\times10^{-4}$ $(300\sim50)$	22, 24, 25
KCl:Tl	10^{-8}	Longer than 2×10^{-3}	$10^{-7}\sim2\times10^{-3}$ $(300\sim50)$					22, 24, 25, 40

TABLE IX. Activation energies for the nonradiative transition, $fT(\Gamma_1^-) \to T(\Gamma_4^-)$.

	°K	meV
KI:Ga	3.3	0.28
KI:In	11.0	0.95

that $\tau_{\mathrm{nonrad}}[fT(\Gamma_1^-) \to T(\Gamma_4^-)]$ is proportional to $e^{\Delta E/kT}$. It should be noted that the nonradiative transitions occur between the particular minima because the $T(\Gamma_4^-)$ and $fT(\Gamma_1^-)$ minima are close to each other as shown in Fig. 7. Therefore, it is reasonable that correlation of polarization is observed between the A absorption and the slow component of the A_T emission.[40,42,43] It is worthwhile noting that the saturation of the decay time is observed below 4°K in KI:In. Two causes are conceivable for the saturation. One is the saturation of the nonradiative transition $\tau_{\mathrm{nonrad}}[fT(\Gamma_1^-) \to T(\Gamma_4^-)]$ and the other is the occurrence of the radiative transition, $fT(\Gamma_1^-) \to \Gamma_1^+$.[25,43] The radiative lifetime 10^{-3} sec may be as long as the order of magnitude of $\tau_{\mathrm{rad}}[fT(\Gamma_1^-) \to \Gamma_1^+]$.

As the temperature is raised above 40°K, the A_X emission begins to increase at the expense of the A_T emission. This is due to the nonradiative transition $T(\Gamma_4^-) \to X(\Gamma_4^-)$ or $fT(\Gamma_1^-) \to eT(\Gamma_1^-)$. In the case of KI:Ga and KI:In, $\tau_{\mathrm{nonrad}}[fT(\Gamma_1^-) \to eT(\Gamma_1^-)]$ is observed in the decay time above about 40°K, because most of the system falls into the $fT(\Gamma_1^-)$ minima. In the case of KI:Tl and KBr:Tl, on the other hand, $\tau_{\mathrm{nonrad}}[T(\Gamma_4^-) \to X(\Gamma_4^-)]$ may be important, because most of the system does not fall into the $fT(\Gamma_1^-)$ minima. Moreover, in the case of KI:Tl and KBr:Tl, there is no positive indication that the fT minima exist on the Γ_1^- APES close to the T minima on the Γ_4^- APES, because the polarization of the slow component of the A_T emission has not been observed.

Now let us consider the A_X emission. In the case of KI:Ga and KI:In, the decay time of the A_X emission is scarcely dependent on temperature and is rather long as shown in Table IV. This is due to the fact that, near at the X minima, the mixing of wave functions occurs between $\Gamma_5^-({}^3T_{1u})$ and $\Gamma_4^-({}^3T_{1u})$. Note that, near at the T minima, no mixing occurs as is clear in Fig. 3. The decay time is determined by $\tau_{\mathrm{rad}}[X(\Gamma_4^-) \to \Gamma_1^+]$ in the temperature region where the A_X emission mainly appears; hence the slow component could not be observed. At lower temperatures, $\tau_{\mathrm{nonrad}}[eT(\Gamma_1^-) \to X(\Gamma_4^-)]$ becomes longer than $\tau_{\mathrm{rad}}[X(\Gamma_4^-) \to \Gamma_1^+]$, and the slow component of the A_X emission may be observed. Since the A_X emission is excited only weakly in the A absorption at low temperatures, it is interesting to measure the decay time by exciting in the C or D absorption and try to obtain the $\tau_{\mathrm{nonrad}}[eT(\Gamma_1^-) \to X(\Gamma_1^-)]$. In the case of KI:Tl and KBr:Tl, $\tau_{\mathrm{rad}}[X(\Gamma_4^-) \to \Gamma_1^+]$ is as short as $\sim 5\times 10^{-8}$ because of the mixing of the $\Gamma_4^-({}^1T_{1u})$ state due to the large spin-orbit interaction (the breakdown of the Russell-Saunders coupling). Hence the slow component is observed, of which decay time is determined by $\tau_{\mathrm{nonrad}}[eT(\Gamma_1^-) \to X(\Gamma_4^-)]$.

D. Polarization

The correlation of polarization between the A absorption and the A_T emission has been observed in Tl^+-type centers in several alkali halides.[7,19,27,31–33] Characteristic features of the correlation are summarized as follows: (1) The azimuthal dependence in the (100) plane becomes zero in the [011] direction.[7,19,27,33] (2) The spectral dependence of polarization is observed within the A-absorption band. The degree of polarization increases as the photon energy of exciting light decreases and approaches some constant value much less than unity (e.g., 0.3).[7,19,27,33] (3) In the case of KCl:Tl, both of the fast and slow components are polarized. The polarization of the slow component quenches at lower temperatures than that of the fast component.[42,43] (4) Thermal quenching of the polarization occurs suddenly in the case of KI:Tl and KBr:Tl, while it occurs by two steps in the case of KCl:Tl.[33,44]

The characteristic features (1) and (2) has already been explained in Ref. 7. Feature (3) results from the fact that the barrier for the nonradiative transition

$$T_z(\Gamma_4^-) \to T_x(\Gamma_4^-) \text{ or } T_y(\Gamma_4^-)$$

is higher than that for

$$fT_z(\Gamma_1^-) \to fT_x(\Gamma_1^-) \text{ or } fT_y(\Gamma_1^-).$$

Feature (4) is closely connected with feature (3). Since in the case of KI:Tl and KBr:Tl no slow component has been observed, the thermal quenching of the polarization is caused only by the nonradiative transition

$$T_z(\Gamma_4^-) \to T_x(\Gamma_4^-) \quad \text{or} \quad T_y(\Gamma_4^-).$$

In the case of KCl:Tl, on the other hand, the quenching is caused by the two kinds of nonradiative transitions and the barriers for them are different from each other as stated above. Thus the quenching occurs by two steps.

Now let us consider why the correlation of polarization between the A absorption and the A_X emission has not been observed so far. The following three reasons are conceivable: (1) The intensity of the A_X emission is several hundredths of that of the A_T emission at low temperatures. The low intensity makes it difficult to detect the small polarization because of the poor signal-to-noise ratio. (2) There are six equivalent X

[42] M. Tomura and H. Nishimura, J. Phys. Soc. Japan **20**, 1536 (1965).

[43] M. Tomura, H. Nishimura, and Y. Kawashima, J. Phys. Soc. Japan **21**, 2081 (1966).

[44] M. Spiller, W. Dultz, and W. Gebhardt, in Ref. 17, p. 262.

TABLE X. The Zeeman interaction matrix. Here g_{orb} is defined by $\langle t_{1u,y}|1_z|t_{1u,x}\rangle = ig_{\text{orb}}$.

				Γ_1^-	Γ_4^-			Γ_3^-		Γ_5^-			Γ_4^-		
$^3T_{1u}$		Γ_1^-	$\frac{1}{\sqrt{3}}(X_-\Theta_x + Y_-\Theta_y + Z_-\Theta_z)$	0	0	0	$\frac{2\sqrt{2}}{\sqrt{3}}\left(1 - \frac{1}{2}g_{\text{orb.}}\right)\mu H$	0	0	0	0	0	0		
	A	Γ_4^-	$\frac{i}{\sqrt{2}}(Z_-\Theta_y - Y_-\Theta_z)$	*	0	$-i\left(1 + \frac{1}{2}g_{\text{orb.}}\right)\mu H$	0	0	0	0	$\left(1 - \frac{1}{2}g_{\text{orb.}}\right)\mu H$	0	0		
			$\frac{i}{\sqrt{2}}(X_-\Theta_z - Z_-\Theta_x)$		$i\left(1 + \frac{1}{2}g_{\text{orb.}}\right)\mu H$	0	0	0	0	$\left(1 - \frac{1}{2}g_{\text{orb.}}\right)\mu H$	0	0			
			$\frac{i}{\sqrt{2}}(Y_-\Theta_x - X_-\Theta_y)$		0	0	0	0	$\frac{2}{\sqrt{3}}\left(1 - \frac{1}{2}g_{\text{orb.}}\right)\mu H$	0	0	0			
	B	Γ_3^-	$\frac{1}{\sqrt{2}}(X_-\Theta_x - Y_-\Theta_y)$	0	*			0	0	0	0	$-2i\left(1 + \frac{1}{2}g_{\text{orb.}}\right)$	0		
			$\frac{1}{\sqrt{6}}(2Z_-\Theta_z - X_-\Theta_x - Y_-\Theta_y)$					0	0	0	0	0			
		Γ_5^-	$\frac{1}{\sqrt{2}}(Y_-\Theta_z + Z_-\Theta_y)$	0	*			0	0	0	$i\left(1 + \frac{1}{2}g_{\text{orb.}}\right)\mu H$	0	0		
			$\frac{1}{\sqrt{2}}(Z_-\Theta_x + X_-\Theta_z)$					0	0	$-i\left(1 + \frac{1}{2}g_{\text{orb.}}\right)\mu H$	0	0			
			$\frac{1}{\sqrt{2}}(X_-\Theta_y + Y_-\Theta_x)$					$2i\left(1 + \frac{1}{2}g_{\text{orb.}}\right)\mu H$	0	0	0	0			
$^1T_{1u}$	C	Γ_4^-	$X_+\Theta_0$	0	0			0		0			0	$-ig_{\text{orb.}}\mu H$	0
			$Y_+\Theta_0$										$ig_{\text{orb.}}\mu H$	0	0
			$Z_+\Theta_0$										0	0	0

minima, while there are only three equivalent T minima. Thus it is more difficult to populate a particular X minimum preferentially than to populate a particular T minimum. Hence the smaller polarization is expected for the A_X emission than for the A_T emission. (3) The A_X emission is efficiently excited in the high-energy part of the A-absorption band. The high-energy excitation may result in the small polarization as explained in Ref. 7.

E. Stress, Stark, and Zeeman Effects

Stress effects on the A_T emission has been investigated in detail by Shimada and Ishiguro[33] and also by Spiller *et al.*,[44] who explained successfully their results in terms of the JTE. Shimada and Ishiguro also studied stress effect on the A_X emission. They concluded that there exist at least two equivalent minima responsible for the A_X emission and that the symmetry of the minima is not tetragonal. These conclusions do not contradict the prediction of Sec. IV. Fontana and Davis[45] have investigated the Zeeman effect of the relaxed excited states of Tl^+ in KI through the analysis of the magnetic-field-induced circular polarization (CP) of the A_T and A_X emission. They found that CP of the A_X emission is large whereas that of the A_T emission is small. They concluded that the excited state responsible for the A_X emission is a nearly degenerate level E_u. Table X shows the Zeeman interaction matrix H_z when a magnetic field is applied in the z direction.[34] The problem is to diagonalize the matrix $H_{el}+H_{so}+H_z$ near the T and X minima. It is difficult to solve the problem, because exact position of the X minima is not known. It is easy, however, to show that $\Gamma_4^-(Z_-\Theta_y-Y_-\Theta_z)$ and $\Gamma_4^-(X_-\Theta_z-Z_-\Theta_x)$ in Fig. 3 or Fig. 7 is split by H_z and that the splitting is not linearly proportional to the strength of applied magnetic field. Thus the experiment by Fontana and Davis is, at least qualitatively, consistent with the theoretical prediction. The Stark effect of the relaxed excited states of Tl^+ in KBr has recently been observed by Giorgianniti *et al.*[46] The observed Stark effect ($\Delta I/I\sim10^{-4}$) is three orders of magnitude as small as the observed Zeeman effect ($\Delta I/I\sim10^{-1}$). This is probably due to the fact that magnetic field splits degenerate $\Gamma_4^-(Z_-\Theta_y-Y_-\Theta_z)$ and $\Gamma_4^-(X_-\Theta_z-Z_-\Theta_x)$ levels ($J=1$, $M=\pm1$) but electric field does not. At all events, these effects seem to be explained by considering the JTE within the $a_{1g}t_{1u}$ electron configuration, though detailed treatment has not been made.

[45] M. P. Fontana and J. A. Davis, Phys. Rev. Letters **23**, 974 (1969).

[46] V. Giorgianni, V. Grasso, and P. Perillo, Phys. Rev. Letters **23**, 640 (1969).

VI. CONCLUSION

It was firmly established that the emission spectra excitable in the A-absorption band of Ga^+, In^+, and Tl^+ in KI, KBr, KCl, and NaCl are explainable within the $a_{1g}t_{1u}$ configuration. There exists no positive reason to introduce other excited states such as an exciton perturbed by adjacent impurity ion originally proposed by Illingworth[22] and supported by Donahue and Teegarden.[23] The apparent complexity of the emission spectra is caused by the spin-orbit and electron-lattice interactions. The problem is to know the APES of the excited states (Γ_1^-, Γ_4^-, etc.) arising from the $a_{1g}t_{1u}$ electron configuration. The Γ_4^- and Γ_1^- APES's were examined by assuming the Russell-Saunders coupling, the linear electron-lattice interaction, and the existence of tetragonal minima. It became clear that there exist two kinds of minima, T (tetragonal) and X (less than tetragonal). The relative depths of the T and X minima vary with the value of $12\zeta(1-\beta)/b^2$, where ζ is the spin-orbit interaction parameter, b is the electron-lattice interaction with the ϵ_g mode, and β is the difference in force constant between exciting and ground states. Three typical cases are distinguished: (1) The depth of the X minima are sufficiently deeper than that of the T minima. (2) The depth of the X minima is nearly equal to that of the T minima. (3) There exists no X minima. Thus we can explain why there exist the three groups of emission spectra represented by KI:Tl, KBr:Tl, and KCl:Tl, respectively. In addition, we can qualitatively explain the characteristic features of the emission spectra, excitation spectra, decay times, and polarization as summarized in Secs. V A–V D. It seems also to be able to explain several data of the stress, Stark, and Zeeman effects obtained recently by various investigators, though detailed analysis has not yet been made.

ACKNOWLEDGMENTS

The author wishes to thank Dr. K. Cho, Dr. M. P. Fontana, Dr. W. Gebhardt, and Dr. T. Shimada for helpful discussions.